Monte-Carlo Based Characterization of the Counting Rate (NECR) Response for Personalized Optimization of the Administered Activity in Clinical PET Imaging

Nicolas A. Karakatsanis[1,2*], George Loudos[3], Arman Rahmim[1,4], Konstantina S. Nikita[2]

1. Division of Nuclear Medicine, Department of Radiology, Johns Hopkins University, USA.
2. Department of Electrical and Computer Engineering, National Technical University of Athens, Greece.
3. Department of Biomedical Technology Engineering, Technological Educational Institute of Athens, Greece.
4. Department of Electrical & Computer Engineering, Johns Hopkins University, USA.

Article info:
Received: June 30 2013
Accepted: September 18 2013

Keywords:
NECR,
Dose,
Optimization,
PET,
Protocol.

ABSTRACT

Purpose: The statistical quality of a PET scan can be significantly affected by the associated patient and scanner characteristics. Standard protocols could be optimized by regulating the administered activity A_{adm} such that the statistical quality is maximized for each individual patient for a given scan time. The objective is to model the direct relationship between the noise equivalent count rate NECR and A_{adm} for a wide range of scanner and patient parameters employed in clinical scans.

Methods: A series of extensive and validated Monte Carlo simulations is utilized to systematically investigate, under realistic and controlled conditions, the effect of a wide set of (i) phantom sizes modeling children, slim and obese patients, (ii) bed positions, (iii) energy windows, (iv) coincidence time windows, (v) and combination of dead times and detector responses on the NECR for a range of A_{adm}.

Results: A wide plateau is observed in NECR(A_{adm}) curves particularly for large patients, suggesting that 90-95% of peak NECR can still be obtained with considerably less A_{adm}. Moreover, for default scanner configurations and cardiac beds, an optimal A_{adm} range of 55-65 MBq for HR+ and 300-450 MBq for Biograph scanners, with the maximum NECR being considerably higher for the latter.

Conclusions: The generalized NECR(A_{adm}) model can be utilized to predict for each individual patient scan an optimal range of A_{adm} for which NECR is maximized, thus potentially allowing (a) for efficient utilization of the available activity in PET centers and (b) for minimization of cumulative radiation exposure.

1. Introduction

1.1. Background

Positron Emission Tomography (PET) imaging has been established in the clinical setting for diagnosis, staging, restaging and treatment response monitoring of a wide range of oncologic malignancies [1-3]. A set of well-defined and streamlined PET data acquisition protocols have been standardized to ensure stability and easy clinical adoption of whole-body PET scans. One of the major objectives of a PET acquisition protocol optimization study is to minimize the impact of noise and, thus, improve the statistical quality of the acquired projection data, by increasing the number of true

**** Corresponding Author:***
Nicolas A. Karakatsanis, PhD
Division of Nuclear Medicine, Department of Radiology, Johns Hopkins University, Baltimore, MD, 21287, USA.
Tel: +1 410 614 1738
E-mail: nicolas.karakatsanis@gmail.com

coincidence counts relative to prompt counts, i.e. the sum of true, scatter and random coincidences counts [4-10]. Effectively, the product of true coincidences with the fraction above denotes the number of "statistically useful counts" in the raw projection data. However, for a given activity distribution, the number of statistically useful counts and, thus, the statistical quality of the acquired projection data does not only depend on the acquisition protocol but also on the properties of the particular patient and scanner [2, 6, 8, 11, 12]. Alternatively, certain studies aimed at image-based optimization of PET acquisition protocol by assessing the noise and lesion detectability in the reconstructed images instead of the statistical quality of the raw projection data [13-16]. Recently, Chang et al. [17] assessed protocol performance in both projection and image domains for various scanner types.

For this reason, PET acquisition protocols are usually customized according to a set of default technical specifications for each scanner in an effort to ensure scanner-tailored acquisitions of overall good statistical quality across multiple bed positions. However, customizations tailored for a fixed set of default parameters may not be adequate enough in the case of certain studies necessitating the tuning of certain technical parameters of a scanner, such as the energy window. Ideally, a more generalized framework should be preferred, capable of accounting for a wide set of possible technical specifications, such as the dead time, the coincidences time window and the detectors type, covering most of the configurations currently applied in modern clinical PET scanners. In addition, the attenuation properties of the imaging subject may vary significantly across patient population, thus resulting in different effects on statistical quality of each scan. Furthermore, if the protocol involves a specific bed position, the corresponding activity distribution properties may differ significantly from the average properties across whole-body field-of-view (FOV). Therefore, in order to optimize the acquisition protocols in clinical human PET studies on an *individualized* scan basis, it is necessary to systematically investigate the effects of a wide set of scanner- and patient-specific parameters on the statistical quality of acquired PET data.

1.2. Focus of the Present Study

In general, two of the most important acquisition protocol parameters affecting statistical quality are the initial amount of administered activity into the patient and the scan time. In the current study, we focus on the optimization of the administered activity level for each patient-specific scan, assuming a constant acquisition time per bed, as determined by the corresponding standard protocol. A reason for this decision originates from the observation that many acquisition protocols rely on constant bed frame durations to streamline and standardize the acquisition process in a routine clinical environment, while less attention is exercised in the personalized regulation of administered activity, which can be more straightforward in terms of clinical implementation.

The metric of noise equivalent counts (NECs), which we elaborate upon in section 2.1, is employed to quantify the statistical quality of the acquired projection or sinogram data. The number of NECs denotes the minimum required number of non-contaminated (true) coincidences counted from an ideal PET system, within a certain scan duration that would produce a statistically equivalent Poisson noise level as that produced by the prompt coincidence counts acquired by an actual scanner, susceptible to contamination from random and scatter coincidences, within the particular scan time. Essentially, the term "statistically useful counts", as defined earlier, refers to the NECs and is equivalent to the square of the signal-to-noise ratio (SNR) in the PET projection data.

Since the scan time is considered a constant for this study, a more appropriate figure of merit for the statistical quality of the projection data could be the rate at which statistical useful counts or NECs are acquired: the noise equivalent count rate or NECR. The higher the NECR, the more NECs are acquired per unit scan time. NECs and NECR are generally not simple monotonic functions of the intensity of the activity distribution. The relation between the NECR and the administered activity or dose A_{adm}, which is usually proportional to the intensity of activity distribution A_t at time t, is a non-linear curve with a peak at moderate dose levels. For small amounts of administered activity, the NECR increases with A_{adm} until it reaches a plateau peak, while for very large dose levels, NECR levels gradually fall off, due to dead-time and pile-up effects as well as high random coincidence count rates (trues are proportional to the activity distribution A_t , while randoms are proportional to the square of A_t).

1.3. Utility to the Nuclear Medicine Community, and Comparison with Alternative Techniques

The last decade has witnessed an increasing interest by the international nuclear medicine community in the role of the administered dose in the statistical

quality of routine human PET clinical studies. Many nuclear medicine professional organizations, such as the Society of Nuclear Medicine and Molecular Imaging (SNMMI) and the European Association of Nuclear Medicine (EANM), have formed scientific committees with the task to survey existing clinical dose administration protocols and subsequently standardize simple international clinical guidelines regarding *individualized* administered dose regimens based on specific criteria, such as the patient weight, the type of tracer, the acquisition mode (2D or 3D) and the bed acquisition length [18-26]. A very recent survey by Alessio et al. [27] have concluded a wide variety of dosing regimens (fixed, range or weight-based) in 225 and 95 clinical facilities in the Unites States for bone and FDG-whole body PET studies respectively.

A strategy for the optimization of a PET acquisition protocol could involve the estimation of the administered activity/dose A_{adm} for which the relative Poisson noise level is minimized or, effectively, the NECR metric in the acquired projection data is maximized. In order to determine the optimal administered activity (A_{adm_opt}), the NECR(A_{adm}) curve or objective function should be estimated for each individual scan. However, the direct calculation of NECR(A_{adm}) from each patient is not clinically feasible, as it requires the initial administration of a relatively very high amount of tracer activity into the patient and a very long acquisition time to allow for the tracer to decay while scanning for a wide range of activity levels.

The NECR has been included as the recommended counting rate metric in the National Electrical Manufacturer's Association (NEMA 2001) NU 2-2001 performance standards publication. Thus, it has been extensively employed in the past as one of the major performance evaluation surrogates to assess the statistical counting rate capabilities of a wide range of clinical human PET scanners from direct experimental measurements [28-32]. All studies above have employed simplified phantoms of basic geometrical shapes, such as cylindrical phantoms, to approximate the human body attenuating tissues and, later, extrapolate the measurements to human scans. However the attenuating properties of the human body are of high complexity and vary across patient population resulting in considerably different NECR responses. Thus, NECR performance evaluations relying exclusively on simple geometrical phantoms may not be accurate and representative of each patient scan. In an attempt to more reliably extrapolate phantom-derived measurements to human clinical environments Smith and Karp [33] measured the prompt and true coincidence rates as a function of the singles rate for both phantom and clinical scans and observed a correlation.

Lartizien et al. [11] developed a method to evaluate clinical patient data based on the counting rate (NECR) curves as derived from prompts and randoms instead of true and randoms rates. Based on phantom measurements, they derived a relation between NECR and the singles rate s but did not attempt to extrapolate NECR curves to individual patient scans. The singles rate s defines the rate of individual events detected before it is determined whether each of these events coincides with another to constitute a coincidence pair of events. As a result, s rates depend on each patient's activity and attenuation distribution properties. However, we note that the coincidence events rate is a function of the given singles events (s) and does not further depend on patient characteristics, which have already affected the s distribution. This observation is utilized in the following studies.

Thus, Watson et al. [34] first demonstrated the counting rates in human subjects could be indirectly estimated by appropriately scaling phantom-derived true, randoms and NECR functions of s to the corresponding data points of individual clinical scans, based on their individual s rates. The scaling is possible as the phantom derived counting rate functions of s are patient-independent and may only be affected by the scanner current configuration. However, the previously estimated patient-specific NECR was termed pseudo-NECR by the authors, as it did not accurately accounted for patient-specific scatter and randoms fractions, because they were not provided by the clinical scanner software at the time. Expanding this concept, Watson et al. [6] proposed a method to indirectly estimate a more accurate patient-specific NECR($A_{adm)}$ response, based on an experimental phantom-derived NECR(*s*) function as well as singles, true, randoms and scatter coincidences obtained from a single patient scan. Thus, they could potentially identify a range of administered activity levels A_{adm} for which the NECR is nearly maximal. Moreover, they applied their method on 2 scanners, each involving 163 clinical FDG PET/CT scans, and evaluated the effect of patient weight and scanner type on the NECR and the optimal A_{adm} range (A_{admopt}). Walker et al. [12] further expanded this methodology to make it applicable to dynamic PET studies by extrapolating to *individualized* NECR(A_{adm}) curves for each dynamic frame. Subsequently, A_{adm} was optimized such that the NECR was maximized within the time frame for which the kinetic parameter estimation was most sensitive. All previous three methods employ an experimental study

involving a geometrical phantom to extract the object-independent NECR(*s*) response of the particular PET scanner. Thus, they only evaluate the overall effect of the scanner configuration on the NECR(A_{adm}) and the A_{adm_opt}. As a result, for every scanner configuration, that could possibly be utilized by the various clinical protocols of every PET scanner model, the phantom study has to be repeated and the respective counting rate models must be rebuilt.

The NECR modeling methods of the previous paragraph were all relying on the relationship between NECR and detector singles rate measurements to build a counting rate response model. In the mean time, Stearns [35] proposed an alternative method to estimate for each patient the full shape of acquisition specific NEC (AS-NEC) curves from the prompts and random counts of a single reference scan of the patient. However, their extrapolation of the NECs to each individual patient scan was based, not on the singles rate, but on the detectors dead-time measurements, as provided by the PET scanner system. Later, Danna et al. [36] implemented and validated the method on the GE Discovery ST PET scanner for a wide set of patients.

The two previous classes of methods are retrospectively predicting patient-specific NECR(A_{adm}) responses relying on specific phantom or clinical measurements and, thus, their examined parameter space is always limited to a particular patient scan. On the other hand, simulations may provide a more standardized and optimizable framework to essentially construct a generalized NECR response model, as they can allow for systematic evaluation of the NECR behavior across a large parameter space. As a result, the previous methods cannot be used to (i) directly relate NECR with A_{adm}, (ii) *prospective*ly optimize the A_{adm} prior to a patient scan, or (ii) alternatively optimize other acquisition parameters itself, such as scan time, energy window etc.. For that, a more systematic investigation has to be conducted regarding the effects of a wider range of scanner- and patient-specific parameters on NECR(A_{adm}) and A_{adm_opt} in order to construct more generalized models that would account for most of the patient study conditions commonly existing in clinical PET imaging.

1.4. Benefits of the Monte Carlo (MC) Approach

Recently, Boldys et al. [37] employed Monte Carlo (MC) simulations to model the NECR(A_{adm}) response for a range of simplified cylindrical phantoms designed to approximate slim and obese patients. They used a specific MC model of a human PET scanner, though its NECR performance was not validated against experimental data as obtained from an actual scanner. Their target was to determine optimal A_{adm} levels such as to ensure uniform statistical quality, as quantified by the acquired number of NECs within a given scan time, for a range of simulated cylindrical phantoms. Thus, they did not focus on maximization of the NEC rate and instead investigated the effect on NECs of subject-related parameters using geometrical approximations of the human torso.

Validated Monte Carlo (MC) simulations, on the other hand, are capable of (i) building accurate models of commercial PET scanners, when combined with highly detailed (voxelized) anthropomorphic phantoms, and (ii) providing a controllable environment to systematically evaluate NECR(A_{adm}) performance under realistic conditions for a large set of possible scanner- and patient-related properties commonly found in PET clinic scans. Previously, numerous NEMA-based performance evaluation studies have been conducted using well-validated MC simulations for various human PET scanners [38-40].

In the current study we utilize a subset of previously validated MC models of commercial PET/CT human scanners to build generalized MC-based counting rate response models capable of accounting for a wide range of possible parameters, such as the patient size, the bed FOV, the energy and coincidence time window, the dead time and the type of detectors. Our MC models have been previously validated against experimental data for a set of performance evaluation metrics, including NECR [38, 40], according to the standards described in NEMA NU 2-2001 guidelines (NEMA 2001) [41]. The construction of the models was made possible thanks to the unique ability of MC simulations to systematically and conveniently reproduce realistic NECR(A_{adm}) functions for a wide range of possible clinical PET imaging conditions. As we have already demonstrated in preliminary studies [8, 9, 42], the produced MC-based NECR response models can help determine not just the NECR(*s*) where is the patient-independent yet scanner -specific singles rate, but also the direct relation of NECR with A_{adm} for an extensive set of important scanner- and patient-specific acquisition parameters, a powerful feature for NECR-driven optimization of acquisition protocols.

Thus, the proposed method has the capability to (i) complement or even potentially replace the phantom-derived NECR(*s*) responses, as utilized by previous studies [6, 12], with more generalized and complete

MC-based NECR(s) models applicable to a wide set of possible scanner configurations, but also (ii) to directly model *individualized* NECR(A_{adm}) curves, effectively removing the need for conducting experimental phantom studies and for modeling NECR(s) responses. Therefore, MC-based generalized NECR response models may potentially facilitate *individualized* and *prospective* prediction of optimal administered dose or acquisition time in the future.

2. Counting Rate Response Model

2.1 Noise Equivalent Count Rate (NECR)

The Noise Equivalent Counts (NECs) concept was first introduced by Strother et al. [43] to describe the equivalent number of counts needed by an ideal imaging counting system to produce the same Poisson noise levels in the measurements as does an actual system that is susceptible to contaminations in the counts. The NEC performance evaluation index is commonly employed in PET imaging to produce the number of counts in the projection data recorded by an ideal PET system, i.e. a hypothetical scanner that records only true coincidences (trues), to produce equivalent Poisson noise levels as produced by the actual PET scanner whose measurements are contaminated with scatter and random coincidences. The NECR is the rate, at which NECs are recorded, mathematically defined by the following equation [32]:

$$\mathrm{NECR} = \frac{T^2}{T + S + (k+1)R} \tag{1}$$

where T, S and R are the average rates of true, scattered and random coincidence events respectively. The value of parameter k is determined by the random coincidences (randoms) estimation method and is assigned the value of 0 for noiseless randoms estimation (via the singles rate) and 1 for randoms estimation (via unsmoothed or non-interpolated delayed sinogram data). In the current study, we consider k to be equal to zero as the randoms rate is directly estimated from the singles rate in Monte Carlo simulations. Thus, equation 1 can be streamlined as follows:

$$\mathrm{NECR} = \frac{T^2}{T + S + R} \tag{2}$$

The NEC can be considered as directly proportional to the square of the signal-to-noise ratio (SNR) of the projection data assuming the measured quantities follow the Poisson distribution, as shown by Watson et al. [44]:

$$\mathrm{SNR}^2_{projData} = \left(\frac{T}{\sigma_T}\right)^2 =$$

$$\frac{T^2}{T + S + (k+1)R}\Delta t = \frac{T^2}{T + S + R}\Delta t = \mathrm{NECR}\cdot\Delta t = \mathrm{NEC} \tag{3}$$

where σ_T is the standard deviation of the trues rate T, and Δt is the acquisition time of the current PET frame. The scattered coincidences (scatters) rate is estimated directly from MC simulations in this study. For systems equipped with LSO detectors, there is a small contribution to the trues, scatters and randoms rates arising from the intrinsic radioactivity of ^{176}Lu, a main component of LSO crystals, which is considered negligible for the activity levels utilized in this study [45].

2.2 The Direct Relationship Between NECR and Administered Tracer Activity

The intensity of the activity distribution at a given bed FOV and a given time frame is determined from the initial level of administered activity, the tracer kinetics of the blood plasma and the tissues included in the bed FOV as well as the decay factor of the radiotracer. Thus, the NECR at a bed position is a function of (i) the administered amount of activity, (ii) the tracer kinetics for the type of organs/tissues included at the bed FOV and (iii) the time relative to injection at which the bed frame is scanned. The decay effect can be easily modeled by applying an appropriate tracer decay factor to all counts of each bed frame and is not further discussed in this study. Moreover, the tracer kinetics can be described by kinetic compartmental models specific for the particular tracer and organ/tissue examined. In the current study we present an example of typical organ-specific tracer kinetics causing non-uniform uptakes between organs of adjacent beds to demonstrate the significance of the resulting kinetic-induced differences in the NECR responses across different beds.

However, our main focus here lies in the effect of the administered activity on the NECR of each individual patient scan. Large amounts of administered activity are most likely to be associated with activity distributions of higher intensity causing higher singles rates, which can actually result in relatively lower NEC performance due to (i) system dead-time and pile-up effects and (ii) much higher randoms rates. On the other hand, moderate amounts of administered activity are usually associated with activity distributions of moderate intensity, resulting in significant reduction of both randoms rate fractions and dead-time effects, thus potentially enhanc-

ing true coincidences rate fractions and NECR performance. Finally, low amounts of administered activity will certainly induce low intensity activity distributions, and thus, low counting rates for singles and all types of coincidences events (trues, randoms and scattered), effectively reducing NECR. As a result, the NECR(A_{adm}) curve of a patient scan usually exhibits a peak at moderate levels of administered activity.

2.3 The $Dose_{90}$ metric and The Range of Optimal Doses

As Watson et al. [6] have observed and our results later confirm, the NECR(A_{adm}) curves exhibit a relatively wide plateau at moderate dose levels. This property of NECR curves suggests that a considerably lower dose can be administered and still obtain an NECR value very close to the peak NECR. In the rest of the study we denote the minimum dose yielding 90% of the peak NECR as $dose_{90}$ and employ it as a complementary metric of $dose_{opt}$ when optimizing the administered dose.

Thus, instead of seeking a particular optimal dose level $dose_{opt}$, a somewhat more practical task would be to determine an optimal range of administered doses, denoted as doserange, and defined as the range of potential administered doses between $dose_{90}$ and $dose_{opt}$, i.e [$dose_{90}$, $dose_{opt}$]. The optimal dose $_{range}$ could be included in future clinical guidelines as a recommendation for a range of possible doses administered to patients of a certain body type to achieve optimal NECR. We should note here that the range [$dose_{90}$, $dose_{opt}$] excludes values corresponding to the declining section of the NECR(A_{adm}) curves, thus ensuring the resulting doses are always at the safe segment of the NECR curves.

3. Simulation Tools

3.1 Monte Carlo GATE Simulations

In the current study, Geant4 Application for Tomography Emission (GATE v6.2), a well validated Monte Carlo simulation package, was employed to model a series of simulated acquisitions of NCAT phantoms of various attenuation and activity distributions [46, 47].

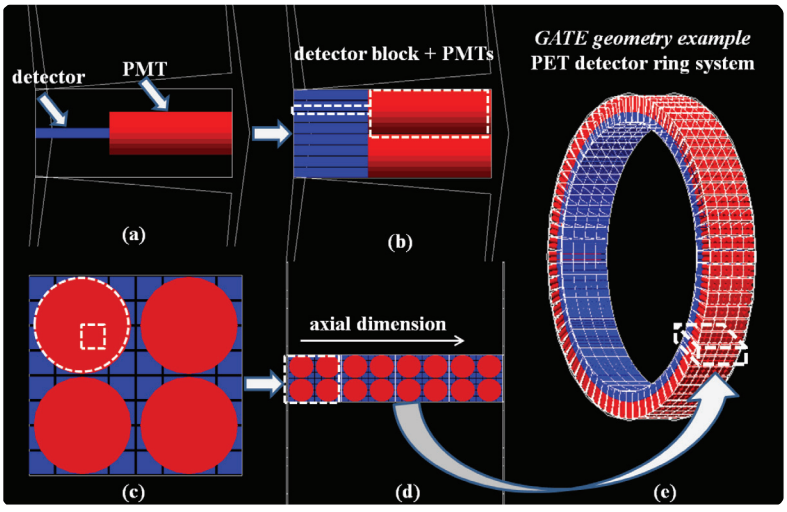

Figure 1. GATE geometry hierarchical levels employed for the building of the GATE model of Siemens ECAT EXACT HR+ scanner. (a) First a single crystal detector and photomultiplier tube (PMT) is built, followed by (b) a repetition over a rectangular grid to form a module consisting of a detector block with four PMTs at the back. The sagittal view of the detector module is shown in (c). Then the module is repeated 4 times along the axial dimension (d) to form a detector head, which, in turn, is repeated in the radial dimension (e) to form the detector ring system.

GATE is based on the well-validated Geant4 simulation toolkit for the accurate modeling of the underlying physics processes taking place in a nuclear imaging study [48, 49]. The Geant4-based software core is expanded with highly customized tools for the detailed hierarchical description of nuclear detector imaging geometries, an example of which is presented for the GATE model of ECAT EXACT HR+ in Figure 1, as well as the control of time-dependent acquisitions and digitizing properties of state-of-the-art PET systems.

GATE platform provides realistic output data in multiple formats. In the current study the list-mode output data in ROOT format have been utilized for the extraction of simulated trues, scatters and randoms rate, from which the NECR can be calculated directly [50]. Moreover GATE offers the ability to control various digitizer, source, timing and geometry parameters of the simulation and determine their independent effect on the NECR of the simulated projection data.

3.2. Voxelized Anthropomorphic NCAT Phantoms

GATE Monte Carlo simulation platform supports both analytical and digital (voxelized) phantoms. In the current study, the NCAT phantom was selected because it supports a homogeneous scaling of the size of all major organs/tissues to reflect the differences in relative body size and geometry commonly observed between patients of different weight [51]. NCAT is characterized by a detailed representation of both the attenuating volume and the activity distribution of the human torso, allowing the accurate modeling of realistic source and material distributions. The phantom has been re-sliced according to the voxel size in all three spatial dimensions, the latter determined from the spatial resolution properties of the Biograph scanner. Subsequently, a set of 64 continuous slices were selected from the bladder to the upper thoracic region in order to cover at least two bed FOVs in the axial direction. Each slice was composed of 96×96 voxels each of. The activity map was generated by initially assigning a uniform background activity concentration over all the tissues of the original phantom followed by replacement of the activity in the regions of the heart, bladder, kidney and spleen with a 32 times higher concentration. As a result, no tracer kinetics has been simulated and the total activity within each bed FOV was determined by the volumes of the tissues included.

The brain was excluded because of its relatively low overall attenuation factor while the bottom part of the body was not modeled to reduce the number of voxels employed in an effort to speed-up the MC simulation. Therefore the activity distributions employed in this study were smaller in size compared to an actual whole-body scan. As a result, given a certain activity concentration for each voxel, the total amount of injected activity is smaller compared to the actual total activity that should have been administered in a patient to drive the same NECR response. Therefore, the total administered dose selected in the simulation was corrected later by a scale factor to reflect a whole-body clinical PET scan. Consequently all the estimated optimal activity ranges were mapped to higher values before being presented in this study.

4. Individualized NECR(A_{adm}) Response

The NECR(A_{adm}) response function of a clinical PET scan can be affected by various (a) scanner and (b) patient-related parameters. The objective in the current study is to systematically investigate, for the first time to our knowledge, the independent effects of such parameters directly on NECR(A_{adm}) performance in the controlled environment of a realistic Monte Carlo simulation set-up. The scanner-related parameters investigated in this study are (a1) the dead-time response of the detector and electronic coincidences system, (a2) the energy window and (a3) the coincidences time window, while the patient-related parameters taken under consideration are (b1) the patient body torso size and (b2) the current bed FOV. The first and second class of examined parameters are summarized in the right and left columns of Table 1 respectively.

Table 1. Examined Parameters Affecting Necr (A_{adm}) Response

Scanner-Related Parameters	Patient-Related Parameters
energy window	body size
dead-time response + type of detectors coincidence time window	bed position/FOV

Each parameter combination essentially defines a potential patient scan. After modeling the NECR(A_{adm}) curves for all possible parameter combinations, one can determine, for each combination, the range of A_{adm} for which the maximum NECR is observed, potentially allowing for truly personalized optimization of administered dose in the routine clinical setting.

4.1. Scanner-Related Effects

In the current study two commercial clinical PET/CT systems of different generations (including different electronic acquisition systems and type of detectors) were considered: the Siemens ECAT EXACT HR+ and the Biograph 6 clinical PET/CT scanners. The respective GATE models of the systems were extensively validated against experimental data [38], as specified by NEMA NU 2-2001 performance evaluation standards [41].

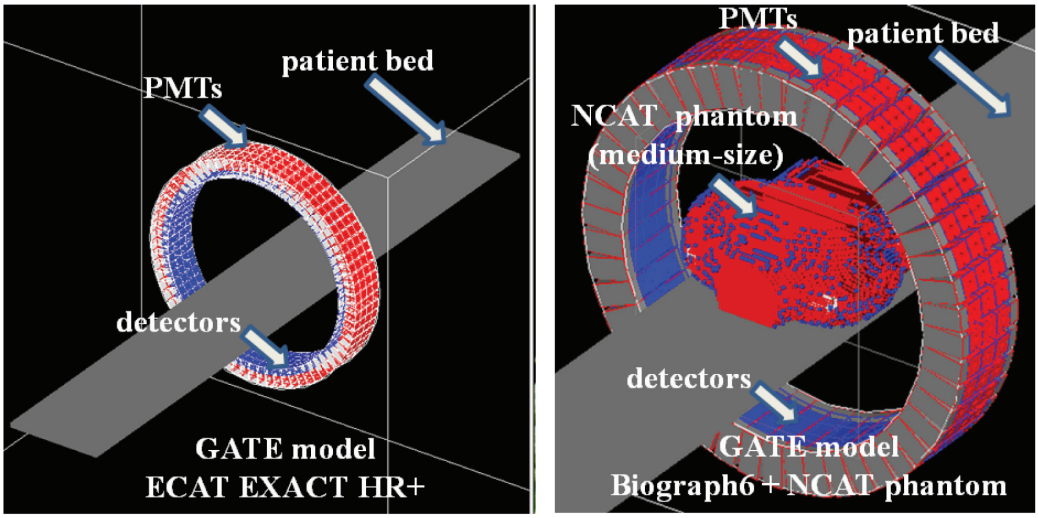

Figure 2. Visualization of the geometry of the GATE model of the clinical PET/CT systems of (a) ECAT EXACT HR+ with the patient bed and (b) Siemens Biograph 6 including the NCAT anthropomorphic voxelized phantom. The right image has been zoomed (zoom factor=2) to better illustrate the relative position and the medium size of the XCAT phantom.

The Biograph 6 scanner is equipped with fast LSO detectors and advanced pico-3D electronics allowing the system to operate with a relative short dead-time detector response. On the other hand, the HR+ scanner utilizes BGO detectors and previous generation electronics and, thus, is characterized by considerably slower dead-time response compared to the Biograph 6 [38]. In Figure 2, the geometric configuration of the two GATE models are presented together with the relative size and position of the voxelized human torso NCAT phantom, by utilizing the GATE visualization tool.

Since the PET acquisition system of the Biograph 6 is characterized by a relatively shorter dead time, it is capable of imaging activity distributions of relatively higher intensity in the 3D mode compared to HR+. Therefore, the NECR metric of HR+ was evaluated for a lower range of administered doses compared to the case of the Biograph, as later presented in the results section.

4.2. Patient-Related Effects

Three characteristic sizes of NCAT phantoms (large, medium and small) were built for the investigation of the body size effect on the NECR. The default lengths of the short and long rib axes of the NCAT original phantom can be modified to homogeneously alter the total size of the phantom. The relative difference between the respective rib axes of each size was set to 15%. Thus, the medium size phantom was generated by employing the default lengths of the NCAT application, while a 15% reduction and increase of the lengths led to the construction of the small and large sizes respectively. The activity and attenuation maps for the three sizes are presented in the left section of Figure 3. The two maps have been fused and presented in the right section of Figure 3 to demonstrate the correct map alignment for each phantom size.

The constructed phantoms resemble characteristic sizes of children (small) as well as slim (medium) and obese (large) adult patients, commonly observed in human population. A total of three sizes were considered adequate for the purposes of investigation of the effect of attenuating volume on the NECR(A_{adm}) responses. However, the proposed methodology does not set a limit on the range of different body sizes that can be examined. For the task of constructing a more generalized NECR response model, a larger variety of body types may be investigated to more accurately project the modeled response to each individual patient scan. In addition, the end-diastole (ED) phase of the cardiac cycle and end-expiration phase of respiration cycle were selected as the single phases for the generation of the NCAT phantoms, as the impact of motion was out of the scope of the current study and was not simulated.

In addition, two bed acquisitions of the same duration (5 min) have been simulated for both systems. Position 1 denotes the bed FOV which includes the heart region at its center, while position 2 refers to the bed position centrally located around the bladder. As we have discussed earlier and also demonstrated by Watson et al. [6], the NECR(A_{adm}) curve varies significantly across different bed positions of the same patient scan, due to the non-uniformity of the activity distribution across the beds, even if the bed frames are of equal time duration. As a result, the NECR of a whole body scan is also expected not to be uniform across beds. An investigation of the effect of bed position on the NECR could be important, as it can potentially assess the significance of the particular effect as well as the importance of this factor when estimating the total administered dose. Thus, in the case of single-bed scans, it may be important to take into account the size of the potential attenuating volume present within the particular bed FOV, for example through a preliminary CT scan prior to the PET scan. Furthermore, in the case of a multi-bed or whole-body PET protocol, a similar calculation may be conducted for each of the scanned bed positions to estimate the total optimal administered dose as the weighted average of the bed-specific optimal dose estimates. For the current study, we have only investigated the effect on bed-specific (not overall whole-body) doses and for two different and characteristic bed positions illustrated in Figure 4.

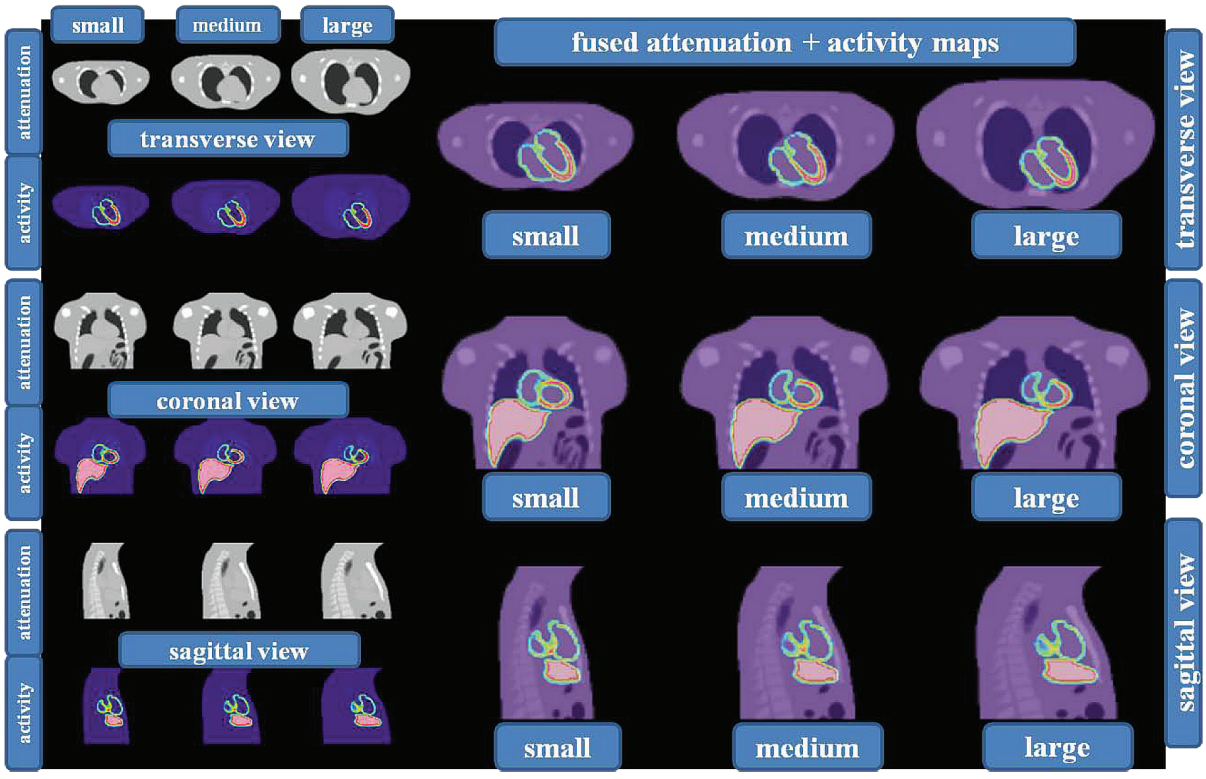

Figure 3. (left hand side) Transverse, coronal and sagittal views of small, medium, and large sizes of attenuation and activity distribution maps of the NCAT human torso phantom. (Right hand side): fused attenuation and activity distribution maps of the left hand side maps. Note on the fused images the correct alignment between the attenuation and activity maps for different sizes.

Certain PET acquisition protocols may require the adjustment of the lower energy threshold (LET) of an energy window to (i) either increase the sensitivity of the system by lowering LET and equivalently allowing a wider energy spectrum or (ii) reduce the scatter contamination induced by low-energy scattered gamma photons by increasing the LET and narrowing the window. Consequently the NECR of a system would be affected accordingly. In this work, three energy windows with a constant upper threshold of 650 keV and varying lower threshold (375, 425, 450 keV) were employed for the LSO scanner and for both bed positions. The LET

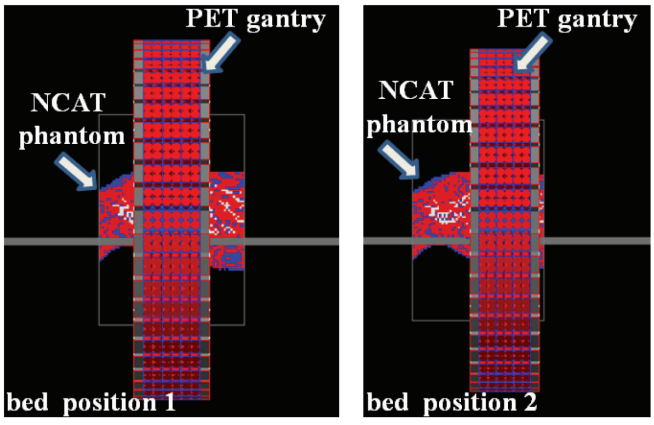

(a) (b)

Figure 4. Sagittal views of (a) bed position 1 and (b) bed position 2 representing the relative axial position of the NCAT phantom with respect to the scanner axial FOV. In both bed positions, the heart and the kidney are located at the center of the axial FOV of the Biograph6 scanner, respectively.

values were selected such as to reflect the most common energy window settings currently employed by various clinical protocols and scanner manufacturers in order to investigate the effect of energy window length and, in particular, of the LET, on NECR and indirectly to the optimal administered dose estimates. The inclusion of the LET factor contributes to the generality of our proposed MC-based NECR(A_{adm}) model and may as well allow for prediction of optimal doses for a larger set of possible scanner settings.

5. Results

5.1. Effect of Body Size on NECR Versus Administered Dose Response

The body or attenuating volume size is the first parameter to be investigated regarding its effect on the NECR(A_{adm}) response model. As the NECR(A_{adm}) curves of Figure 5 illustrate, the counting rate performance of Biograph 6 is enhanced for smaller phantom body sizes for a wide range of administered doses (10-4000 MBq).

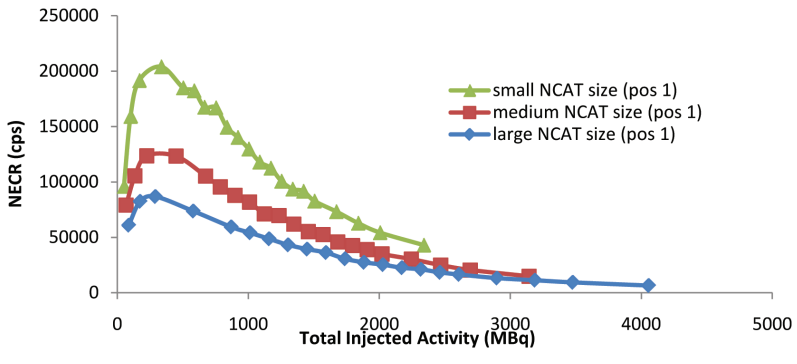

Figure 5. Biogarph NECR vs an extended range of administered dose levels to demonstrate overall effect of phantom body size on NECR response. Three different sizes (small, medium, large) of NCAT phantom sizes, a 425-650 keV energy window and bed position 1 are employed

The results confirm the theoretically expected behavior of NECR for different sizes of attenuation volumes. Smaller phantom sizes are expected to be associated with higher NECR as they provide equivalently smaller attenuating volume sizes and, thus reduced probability of attenuation for each emitted gamma photon. As a

result, smaller subjects result in higher trues fraction, while the scatters and randoms fraction are reduced. On the contrary, larger subjects are expected to exhibit lower NECRs as they are associated with higher probability for attenuation, i.e. less trues and more scatter and random fractions.

In the following sections the administered activity level ranges are limited to 10-1200 MBq for the case of the HR+ and Biograph 6 to better illustrate the behavior of the counting rate response at dose ranges commonly administered into clinical patients. Figures 6 and 7 show the dependence of NECR(A_{adm}) curve for HR+ and Biograph 6 respectively both in the 10-1200 MBq range.

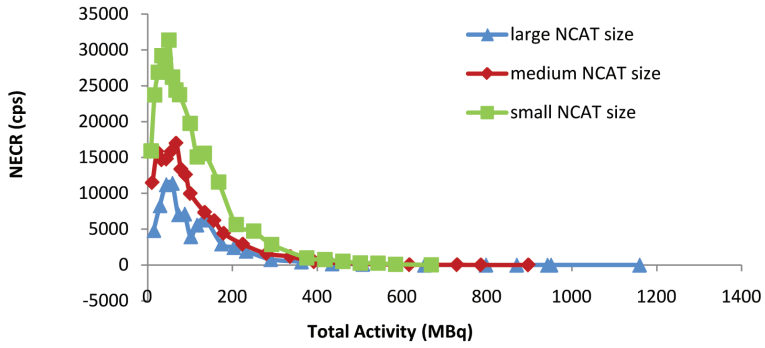

Figure 6. HR+ NECR vs. administered dose for three different sizes (small, medium, large) of NCAT phantom sizes, when a 425-650 keV energy window and bed position 1 is selected

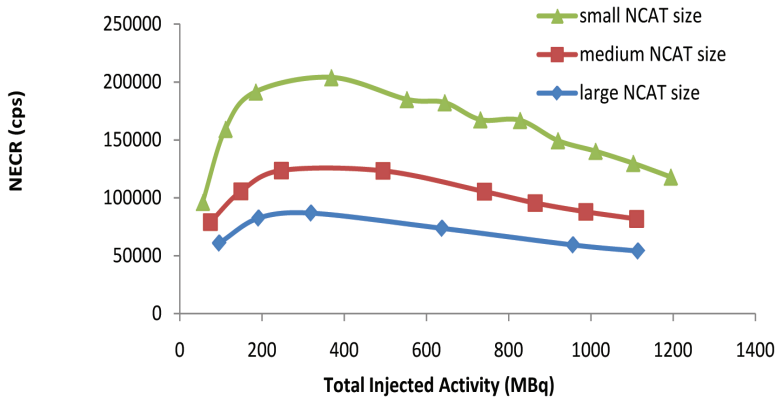

Figure 7. Biograph NECR vs. administered dose when three different sizes (small, medium, large) of NCAT phantom sizes are employed.

The results indicate that the position of peak NECR with respect to the administered dose (x-axis) is somewhat affected by the phantom body size for the case of Biograph 6, with NECR peaking at smaller doses for larger patients. After plotting the optimal dose ($dose_{opt}$) of Biograph 6 versus the three phantom sizes, we observe in Figure 7 a negative linear correlation between them. By contrast, the peak NECR of HR+ is reached at approximately the same dose ranges for the three sizes.

As we have described in section 2.3 and our results demonstrate, the NECR(A_{adm}) curves exhibit a relatively wide plateau at moderate dose levels in all body types and most particularly for larger patients. The wide pla-

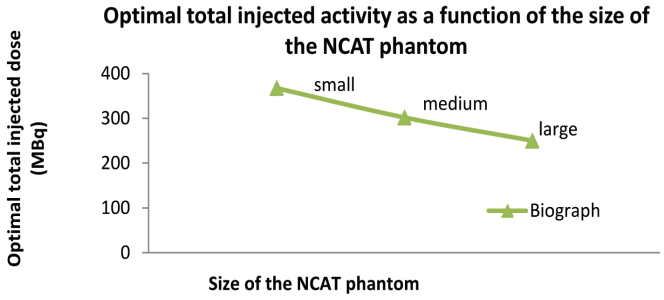

Figure 8. Estimated optimal administered doses ($dose_{opt}$) for Biograph 6 and for three different NCAT sizes based on the previous estimation results of Figure 6.

teau is observed for both HR+ and Biograph scanners (Figure 5 and 6) if we focus on the range of moderate doses, which are usually employed in clinical protocols (Figure 7). This property of NECR curves suggests that a considerably lower dose can be administered and still obtain 90% of the peak NECR. This new dose level, denoted as $dose_{90}$ in section 2.3, also exhibits a negative correlation with the phantom size. However, as suggested from the results in Figures 6 and 7, the optimal $dose_{range}$ for each body size exhibit a high degree of overlap between the three sizes implying minimal dependence to phantom size.

By comparing Figures 6 and 7 we observe that, while in both systems the peak NECR value is strongly affected by the phantom size, the degree to which the optimal dose is affected may be varying, as pointed out in the previous paragraph. We believe the relatively higher counting rate responses, such as that of Biograph 6, are more sensitive to patient attenuating volume sizes and, thus the optimal dose may also exhibit higher degree of correlation in these cases. For HR+, on the contrary, the optimal dose does not appear to be correlated with phantom size.

5.2. Effect of Scanner Properties on NECR Versus Administered Dose Response

In Figure 9 the NECR curves of a large NCAT phantom for the case of the Biograph and HR+ systems are plotted together for comparative evaluation. The maximal NECR for the Biograph 6 scanner is approximately 8 times higher, while the respective optimal dose is 7 times higher. The use of advanced electronics with considerably faster dead-time response allows Biograph 6 to achieve higher NECR performance for the same amount of administered dose. Furthermore, the peak NECR is reached at a significantly higher dose level. The optimal administered dose for the HR+ system lies in the range of 55-65 MBq, while for Biograph the same range is 300-450 MBq.

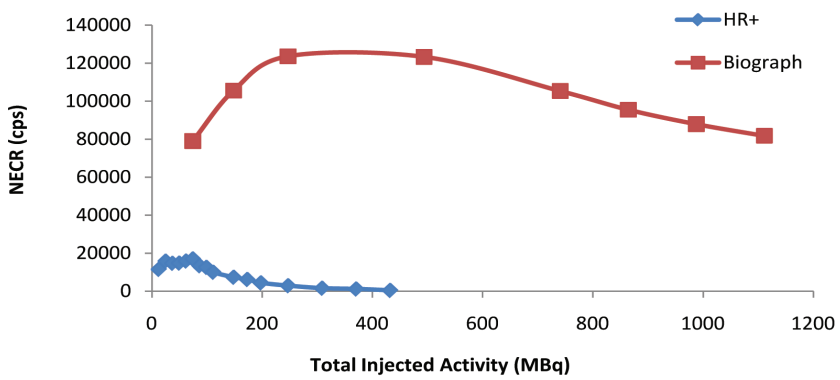

Figure 9. Comparative diagram of the NECR curve vs. administered dose for two commercial PET systems: Biograph 6 (LSO) and HR+ (BGO) scanner. A large NCAT phantom size has been used with an energy window of 425-650 keV, bed position 1 is selected

An energy window of 425-650 keV had been selected for all previous simulation series. In the following section, the low energy threshold (LET) of Biograph 6 window was modified and the respective effects are presented at Figure 10. When the LET is raised from 425 to 450 keV a slightly improved NECR value was measured over the entire range of dose levels. On the contrary, when the LET was dropped down to 375 keV, resulting in a wider energy window, a fall-off in the NECR performance was recorded, due to the higher fraction of scattered and random events compared to trues. On the other hand, the optimal dose range does not appear to be affected significantly by the energy window.

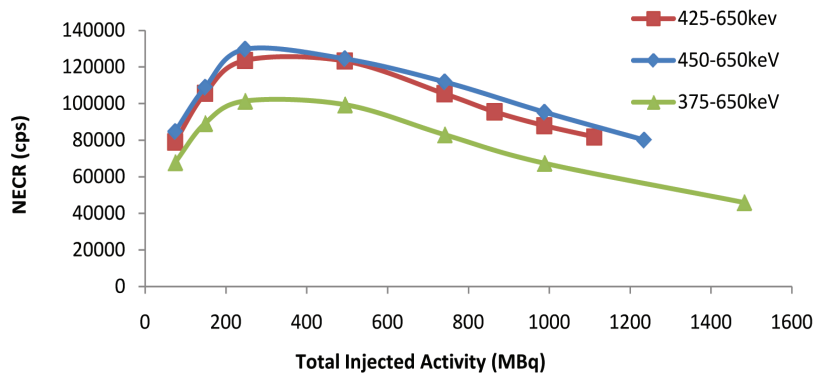

Figure 10. Biograph NECR vs. administered dose for various energy windows. A medium size NCAT and bed position 1 have been selected

The coincidence time window (CTW) determines the maximum allowed time period within which two single events are considered as a single coincidence event by the coincidence sorter module of the PET acquisition system. Every commercial clinical PET scanner is usually characterized by a single CTW in the order of ns and is dependent on certain technical specifications such as the ring diameter, the dead-time and the response of the detectors. Biograph 6 has a CTW of 4.5 ns according to the manufacturer. In order to investigate the CTW effect on NECR, two additional CTW lengths were also simulated with the results shown in Figure 11. The results suggest that a larger CTW will induce a lower NECR response, due to the higher fraction of random coincidences allowed within a larger CTW. Moreover, larger CTW is also associated with smaller optimal doses.

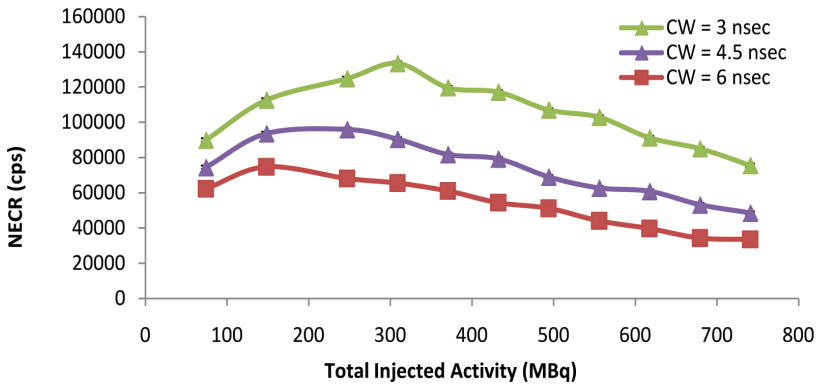

Figure 11. Biograph NECR vs. administered dose for different hypothetical coincidence time windows. A medium size NCAT and bed position 1 is employed.

The axial bed position employed in all previous acquisitions corresponded to position 1, where the heart is positioned at the center of the axial FOV. When position 2 is selected, the high-activity region of the bladder is now at the center of the FOV resulting in 8 times increase of the peak NECR, while the optimal dose rises to ~580 MBq (Figure 12). On the other hand, the HR+ NECR in position 2 becomes 3 times higher relative to position 1, while the optimal dose remains insensitive (Figure 13).

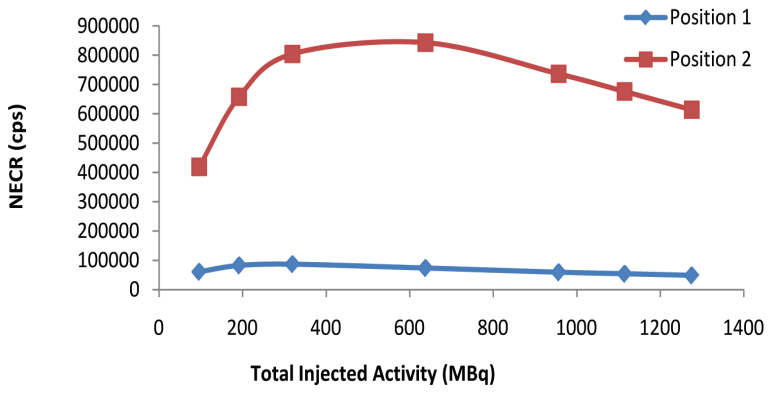

Figure 12. Biograph NECR vs. administered dose when the heart (position 1) or the bladder (position 2) are located at the center of the FOV, the medium size NCAT and the energy window of 425-650 keV has been used

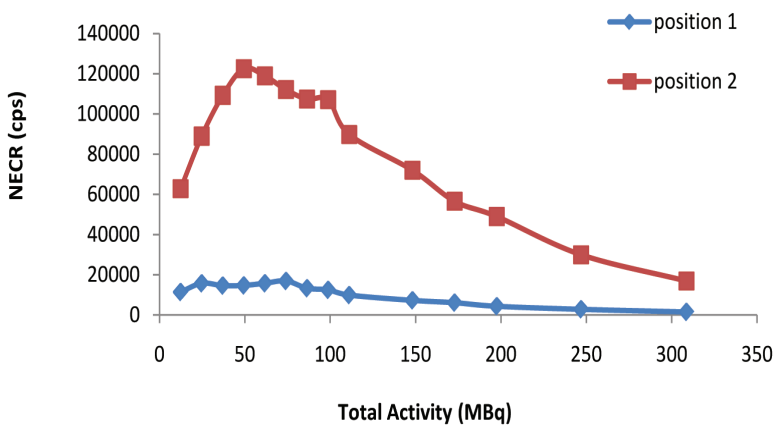

Figure 13. HR+ NECR vs. administered dose when the heart (position 1) or the bladder (position 2) are located at the center of the FOV, the medium size NCAT and the energy window of 425-650 keV has been used.

6. Discussion

6.1. NECR Dependence on Patient Size

For the range of patient sizes examined in this study, we observed a negative correlation between $dose_{opt}$ and patient body size for the Biograph 6 scanner, while almost no correlation was found for the HR+ scanner. However, we believe this does not exclude the possibility of deriving other types of correlations (e.g. positive) for other scanner or patient characteristics. In this point we would like to note that this study is aiming at the proposition of a method to build a generalized MC-based NECR response model that could allow for the prediction of personalized optimal dose amounts for each patient. However, we do not provide here specific dose recommendations as they vary, as our results suggest, for each patient scan. Nevertheless, for the case of Biograph 6 scanner, an indication of recommended $dose_{opt}$ for the three phantom sizes is shown in Figure 8. Also,

$dose_{90}$ was consistently ~100 MBq lower than doseopt. In addition, for the case of HR+ the respective $dose_{opt}$ values were considerably lower, while a distance of ~25 MBq was observed between $dose_{opt}$ and $dose_{90}$.

Regardless of whether a dose optimization strategy is applied or not, an efficient dose regimen should always aim at NECR responses belonging to the inclining section of NECR(A_{adm}) curve, ideally approaching peak NECR from the left. As our results suggest, for patient scans involving systems with faster electronics and detectors or slim adults or children, a standard administered dose is more likely to drive responses to the inclining section of NECR curve. By comparison, a standard dose is more likely to correspond to the declining section of the NECR(A_{adm}) curve when the associated PET systems are characterized by relatively slower electronics or detectors, and possibly when obese or larger size patients are scanned. A dose optimization strategy, as the one proposed in the present study, may help ensure that the standard dose is adjusted such as the driven NECR responses belong to the inclining section of the NECR(A_{adm}) curve in all cases, and with no more than 10% reduction of the peak NECR value ($dose_{90}$). As the image quality of the clinical images is determined, up to a certain degree, by the NECR of the acquired data and not the administered dose, the diagnostic and quantitative value of the images is only expected to exhibit a negligible, if any, degradation when injecting $dose_{90}$ amount of tracer as opposed to a larger dose.

In certain extreme cases, the recommended optimal dose may violate other important requirements. For example, for the class of fast-responding scanner and pediatric patients, an NECR model, like the one proposed in the current study, can result in recommendation of high optimal doses, which, in turn, may enhance the already increased radiation exposure risk associated with small children. A solution to this special case will be to administer $dose_{90}$ or even a dose smaller than optimal to ensure the cumulative exposure risk is limited. Particularly for slim and pediatric patients a sufficient NECR response is obtained for doses smaller than optimal. On the other hand, we note that for very obese patients and slow-responding scanners, even the optimal dose may result in very low NECR responses resulting in insufficient number of NECs for a standard acquisition time. An appropriate elongation of the acquisition to collect sufficient NECs for that frame may provide a solution to this special case. The above recommendations regarding the NECR effects for certain extreme, but not rare, patient scan conditions in clinical PET studies agree with the conclusions of relevant publications [6, 12, 16, 52].

6.2. The Computational Challenge

Moreover, the main objective in the present study is to present a methodology to build MC-based NECR response models and also demonstrate its potentials and future prospects compared to existing methods in terms of NECR-based *prospective* optimization of administered dose in clinical PET scans assuming a standard acquisition time. However, the feasibility of the method relies on the completeness and generality of the MC-based model, which, in turn, depends on the number of dimensions and size of the parameter space investigated. Monte Carlo simulations especially when combined with voxelized finely detailed phantom geometries are overall computationally expensive and an efficient simulation design strategy is necessary to be able to systematically investigate the effect on NECR(A_{adm}) response of a range of parameters. In the current study, GATE simulations have been efficiently distributed, utilizing computing job schedulers, across a pool of 48 CPU cores in an effort to reduce the execution time. The counting rates have been estimated by acquiring data of 5sec acquisition times across a wide range of intensities of two bed NCAT activity distributions. The current method does not impose limitations on the size or sampling frequency of the parameter space examined and, thus, a higher degree of efficiency may potentially further enhance the accuracy of the model.

6.3. Characterization of Individual Patient Anatomies

The effect of patient size on NECR response has been demonstrated by simply varying the overall size of the NCAT human torso phantom. NCAT software supports a uniform and proportional change of volume size of each region to reflect the organ-specific differences between slim, medium and large patients. In reality, though, each patient's geometry is characterized by unique body structure and non-uniform organ volume distribution. As a result, our examined phantom sizes, though they are considered representative, may not accurately reflect the actual attenuating properties of each patient. However, our findings suggest that NECR is not very sensitive to different patient sizes and, thus, the examination of a small range of representative body types should be sufficient.

6.4. Projection-Space vs. Image-Space Noise Analysis

Although NECR is considered a reliable and popular metric of the statistical quality of PET projection data, it has certain limitations that should be acknowledged.

The projection data do not always follow Poisson distribution due to dead-time effects [53], rebinding or correction methods. Moreover, the NECR metric refers to the projection data and not the images necessarily. It does not account for the effects of normalization and attenuation correction, data reconstruction or spatial mispositioning due to detectors pile-up. Watson et al. [44] has shown that the NECR(A_{adm}) response is correlated with the PET image SNR(A_{adm}) response for filtered backprojection reconstruction of Poisson data. On the other hand, a similar correlation has not been confirmed for iterative ordered-subset expectation maximization (OSEM) reconstruction algorithms [54]. Subsequently, caution and further validation may need to be exercised in extending results from projection-space NECR analysis to reconstructed images.

7. Potentials and Future Prospects

7.1. Prospective Individualized Optimization of Administered Amount of Activity

The proposed framework allows for systematic inclusion of a wide range of scanner- and patient-related parameters into the NECR(A_{adm}) response model without the need to conduct phantom or patient reference measurements. As a result, a potentially limitless number of realistic NECR effects for a wide variety of scanners and patient body types can be modeled within a controllable environment to acquire a large collection of simulated data to enhance the completeness and accuracy of the NECR(A_{adm}) model.

Therefore, as a future prospect, a large collection of data can be generated for a wide variety of populations and acquisition parameters, and utilized in the proposed context, to (i) build population-based NECR(A_{adm}) models for characteristic classes of scanners and groups of patient population, (ii) utilize these models for population-based *prospective* optimization of *individualized* A_{adm} and (iii) alternatively optimize other important acquisition parameters such as scan time or energy window.

7.2 Efficient Utilization of Available Radiopharmaceutical Dose

The modeling of NECR(A_{adm}) response and the associated *prospective* optimization of A_{adm} on an *individualized* basis can be very important, as it will allow for more efficient utilization of the daily amount of radiotracer available for administration in PET clinics with high throughput of patients. PET clinical centers usually order a particular amount of various radiotracers on a routine basis, depending on each tracer half-life, to conduct a scheduled series of studies. In addition, many common PET tracers are characterized by relatively short half-lives or high production cost, properties which become even more significant if a cyclotron is not in proximity to the PET scanners. Therefore, the efficient management of the initially available amount of tracers is vital for the cost-efficient operation of a PET center.

A potential solution to the challenge described above could be the NECR-based optimization of the administered amount of activity to ensure for a particular tracer and a given scan period an adequate level of statistical quality with the lowest possible amount of administered activity. However, as we have discussed above, each patient scan is associated with different scanner- and patient-related parameters which, in turn, can drastically affect the NECR, i.e. the statistical quality of the acquired PET data. Therefore, to efficiently manage the available daily amount of tracer in a PET center it is important to conduct an *individualized* regulation of the administered tracer amount.

An alternative strategy to efficiently utilize the available initial tracer amount would suggest the optimization of the total scan time of each patient for a standard administered activity to each patient. Nagaki et al. [55] have conducted a retrospective analysis of 76 patients to optimize the acquisition time for a range of weights based on NECR and coefficient of variance (COV) in liver image regions. Preliminary results from an extension of the current work focusing on scan time optimization have been presented in the past [10]. In this case, MC simulations can provide a suitable and convenient framework to examine a range of different acquisition times that would not have been clinically feasible as it would have required multiple scans for same patients. However, as we have previously explained, in this study we focus on the optimization of the administered tracer amount assuming a standard scan time, as determined by the standard clinical acquisition protocols.

7.3 Minimization of Ionizing PET Radiation Exposure for Pediatric Patients

Recently published PET/CT procedure guidelines from the Society of Nuclear Medicine and Molecular Imaging (SNMMI) and the European Association of Nuclear Medicine (EANM) have demonstrated the importance in patient scan-specific amounts of adminis-

tered activity. Based on extended clinical studies they have standardized simplified mathematical dosage formulas to determine in a routine clinical setting the minimum amount of activity that should be administered to patients based on their weight, the acquisition mode (2D or 3D), the scan time per bed position and in some cases the percentage of bed overlapping. However, the recent technological advances in PET/CT scanners have resulted in higher sensitivity and NECR performances allowing for large safety margins in optimizing administered doses for adult patients and, thus, simple linear models may be adequate for predicting safe doses.

On the other hand, the same technological trend, has encouraged the application of PET and other nuclear medical imaging techniques to pediatric patients even of small age. The effect of the radiation exposure risk for this class of patients may be more drastic and more sensitive and accurate models should be employed to recommend minimum possible amounts of administered PET tracers as a function of the weight and other scan parameters [22, 23, 25-27, 56]. For this reason, PET/CT radiation exposure risk to children has gained considerable interest recently, as suggested by the increasingly larger number of published PET acquisition guideline studies especially for pediatric PET/CT scans [18-21, 24, 57]. Although the main contribution to exposure risks originates from CT radiation, PET emitting radiation is also significant and the principles of As Low As Reasonably Achievable (ALARA) concept should be taken into serious consideration when designing pediatric acquisition protocols [52, 58].

As the results of the current study have demonstrated, patients of small body size, usually representing children, are associated with higher optimal administered doses relative to larger patients, such as obese children or adults. In addition, the scans of the former class of patients are characterized by much higher NECR values, due to smaller degree of radiation attenuation effects. Thus, in those patients a protocol can very effectively afford considerably smaller doses without compromising NECR and statistical quality relative to larger patients. In addition, similarly to obese adult patients, obese children administered with high doses are not necessarily associated with higher NECR than the rest of the children patients, suggesting lower doses and larger scan times, if possible, to ensure high statistical quality.

7.4. Dose Optimization for PET/CT and PET/MR Acquisitions

In the present study we focus on the management of the administered radiopharmaceutical dose in PET clinical studies. However, modern clinical PET imaging systems are also equipped with CT or MRI components for the anatomical characterization of the subject to improve attenuation correction and image quantification. In PET/CT imaging, the CT-related dose effect remains higher than the respective PET-related effect [59], even though low-dose CT features have been standardized in modern PET/CT protocols [60]. Therefore, the optimization process for minimum possible PET dose, though not as significant as for CT dose, would contribute to a certain reasonable extent to the overall reduction of the biologically effective dose for each patient. On the other hand, in PET/MR imaging protocols the ionizing radiation exposure risk is mainly related to PET administered dose only, thus allowing for larger safety margins in dose administration before posing any exposure risks [61- 63]. Therefore, in future we propose also accounting for the dose of CT-related ionizing radiation, when designing optimal PET/CT acquisition protocols. Moreover, in both PET/CT or PET/MR protocol optimization, cumulative radiation exposure must always be taken under serious consideration, especially for pediatric patients or patients undergoing multiple PET scans, for e.g. in the case of treatment response monitoring.

8. Summary and Conclusions

In the current study a methodology has been proposed for the construction of an *individualized* NECR response of clinical PET systems as a function of the administered activity or dose A_{adm}. A systematic investigation of the effect on NECR(A_{adm}) was performed based on parameters of (i) body size, (ii) bed position, (iii) energy window, (iv) coincidences time window, and (v) scanner dead-time response and detectors, for a wide range of possible values.

The combined utilization of accurate Monte Carlo GATE simulations and highly-detailed voxelized NCAT anthropomorphic phantoms enable systematic investigation of the NECR effect due to each of the abovementioned parameters in a controlled environment and for multiple noise realizations. However Monte Carlo simulations tend to be computationally expensive and the feasibility of the presented method relies on efficient simulation configurations that will ensure reasonable execution times for the acquisition

of all necessary simulated data to build an accurate and generalized NECR response model.

The counting-rate response model can *prospective*ly predict the direct NECR(A_{adm}) response of individual patient scans, as it accounts for a wide set of important scanner- and patient-related parameters affecting the statistical quality of acquired PET projection data. In addition, the ability to directly estimate the relationship between NECR and A_{adm} quantities effectively removes the need for conducting additional measurements to project the model-estimated response to individual patient scans. Thus our proposed methodology provides an efficient and clinically feasible solution to the problem of *prospective* optimization of administered dose.

In particular, we have concluded that the NECR is strongly dependent on the size of the patient, the scanner dead-time, CTW and detectors response as well as the bed position and less affected by the energy window length. We have confirmed the theoretic expectation that larger patients would be associated with higher probabilities of attenuation and, therefore higher scatter and random fractions, thus lower NECR performances. Moreover, state-of-the-art PET systems with shorter dead-times and faster detectors or shorter CTWs may achieve considerably higher NECRs for the same dose levels and overall higher peak NECRs. Equivalently, these system may reach the same NECR levels at significantly lower doses. In addition, the bed position affects the NECR and should be considered when a study focuses on a particular (single) bed or when the overall whole-body NECR needs to be calculated from highly variant bed FOVs. Finally, the energy windows commonly employed in the clinic have some impact on NECR with 450-650 keV providing the best performance.

From the three definitions for NECR-based optimal administered dose ($dose_{opt}$, $dose_{90}$ and $dose_{range}$) provided in the current study, $dose_{range}$ is perhaps the most clinically relevant and feasible as it recommends not a specific value but a range of values defined as [$dose_{90}$, $dose_{opt}$]. Within that range of recommended doses, a selection closer to the lower end ($dose_{90}$) of the range should be preferred as it is associated, by definition, with lower amount of doses while not affecting the NECR significantly.

The parameters with the highest impact on all above definitions of optimal doses were the dead-time, the CTW and the detector response followed by the bed position and the body size, while the energy window did not appear to have as significant an impact. Overall, the Biograph 6 scanner, equipped with faster detectors and electronics and, therefore, shorter CTW than HR+ was associated with wider plateau regions and therefore the $dose_{90}$ criterion for optimization becomes more important as the dead-times and coincidence time windows becomes shorter with the advance of technology. In addition, a relatively weak and negative linear correlation was observed between the phantom size and the optimal dose definitions of $dose_{opt}$ and $dose_{90}$, while dose¬range was not affected considerably. These correlations were more evident for systems of higher NECR, such as the Biograph. Furthermore, the degree of attenuation taking place in different bed FOVs can affect the NECR at each bed significantly and therefore a bed-specific dose optimization strategy is highly recommended. Moreover the activity uptake at each bed FOV may be different depending on the tracer kinetics of the respective organs located at each bed FOV.

As we have discussed in the previous section, a desirable and efficient clinical dose regimen should always drive *individualized* NECR(A_{adm}) responses within the inclining section of the NECR(A_{adm}) curve approaching the peak NECR value from the left. The proposed method optimizes administered dose based on this objective exactly. Especially for the parameter of patient size and based on our results it is recommended to administer a limited or reduced dose to very obese patients and scan them longer to acquire a sufficient number of NECs per bed. On the other hand, small children may be administered doses according to the optimized dose regimen of $dose_{90}$ proposed here, providing that the associated radiation exposure risk remains within acceptable limits. Besides, our results indicate that further decrease of the administered dose can be afforded as the attenuation from small body sizes is minimal.

Acknowledgements

The authors would like to thank the OpenGATE collaboration and Dr William P. Segars for allowing us to use the NCAT phantom and GATE simulation software, respectively, for the purposes of this study. We would also like to thank Dr Arion F. Chatziioannou from the Crump Institute of Molecular Imaging, UCLA for all the valuable insight he has provided us throughout this study.

References

[1] Wahl, R.L. (2002). Principles of cancer imaging with fluorodeoxyglucose. In: Wahl, R.L., Buchanan, J.W., eds. Principles and Practice of Positron Emission Tomography. Philadelphia, Pa: Lippincott Williams & Wilkins.

[2] Rahmim, A. and Wahl, R.L. (2006). An overview of clinical PET/CT Iran. Journal of Nuclear Medicine, 14(26), 1-14.

[3] Facey, K., Bradbury, I., Laing, G. and Payne, E. (2007). Overview of the clinical effectiveness of positron emission tomography imaging in selected cancers. Health Technol Assess, 11(44), iii-iv, xi-267.

[4] Lartizien, C., Kinahan, P.E. and Comtat, C. (2004). A lesion detection observer study comparing 2-dimenional versus fully 3-dimensional whole body PET imaging protocols. Journal of Nuclear Medicine, 45, 714-723.

[5] Badawi, R.D., Dahlbom, M. (2005). NEC: Some Coincidences Are More Equivalent Than Others. Journal of Nuclear Medicine, 46(11), 1767-1768.

[6] Watson, C.C., Casey, M., Bendriem, B., Carney, J., Townsend, D., Eberl, L., Meikle, S., DiFilippo, F. (2005). Optimizing injected dose in clinical PET by accurately modeling the counting-rate response functions specific to individual patient scans. Journal of Nuclear Medicine, 46(11), 1825-34.

[7] MacDonald, L.R., Schmitz, R.E., Alessio, A.M., Wollenweber, S.D., Stearns, C.W., Ganin, A., Harrison, R.L., Lewellen, T.K. and Kinahan, P.E. (2008). Measured count-rate performance of the Discovery STE PET/CT scanner in 2D, 3D and partial collimation acquisition modes. Physics in Medicine & Biology, 53, 3723-3738.

[8] Karakatsanis, N., Parasyris, A., Loudos, G. and Nikita, K. (2008b). A Simulation study of the counting rate performance of clinical PET systems applying a methodology for optimizing the injected dose. IEEE Nucl Sci. Symp. Conf. Record, 5014-5019.

[9] Karakatsanis, N., Nikita, K. (2009a). A simulation model of the counting rate response of clinical PET systems and its application to optimize the injected dose. IEEE Int. Symposium on Biomedical Imaging (ISBI), 398-401.

[10] Karakatsanis, N., Loudos, G. and Nikita, K.S. (2009b). A methodology for optimizing the acquisition time of a clinical PET scan using GATE. IEEE Nucl Sci Symp Med Imag Conf, 2896-2901.

[11] Lartizien, C., Comtat, C., Kinahan, P.E. (2002). Optimization of injected dose based on noise equivalent count rates for 2- and 3-dimensional whole-body PET. Journal of Nuclear Medicine, 43, 1268-1278.

[12] Walker, M.D., Matthews, J.C., Asselin, M-C., Saleem, A., Dickinson, C., Charnley, N., Julyan, P.J., Price, P.M. and Jones, T. (2009). Optimization of the injevcted activity in dynamic 3D PET: A generalized approwach using patient-specific NECs as demonstrated by a series of 15O-H2O scans. Journal of Nuclear Medicine, 50(9), 1409-1417.

[13] Everaert, H., Vanhove, C., Lahoutte, T., Muylle, K., Cavaliers V, Bossuyt, A. and Franken, P.R. (2003). Optimal dose of 18F-FDG required for whole-body PET using an LSO PET camera. European Journal of Nuclear Medicine and Molecular Imaging, 30(12), 1615-9.

[14] Halpern, B.S., Dahlbom, M., Auerbach, M.A., Schiepers, C., Fueger, B.J., Weber, W.A., Silverman, D.H., Ratib, O. and Czernin, J. (2005). Optimizing imaging protocols for overweight and obese patients: a lutetium orthosilicate PET/CT study. Journal of Nuclear Medicine, 46(4), 603-7.

[15] Halpern, B.S., Dahlbom, M., Quon, A., Schiepers, C., Waldherr, C., Silverman, D.H., Ratib, O. and Czernin, J. (2004). Impact of patient weight and emission scan duration on PET/CT image quality and lesion detectability. Journal of Nuclear Medicine, 45(5), 797-801.

[16] Masuda, Y., Kondo, C., Matsuo, Y., Uetani, M. and Kusakabe, K. (2009). Comparison of Imaging Protocols for 18F-FDG PET/CT in Overweight Patients: Optimizing Scan Duration vs. Administered Dose. Journal of Nuclear Medicine, 50, 844-848.

[17] Chang, T., Chang, G., Kohlmyer, S., Clark, J.W., Rohren, E. and Mawlawi, O.R. (2011). Effects of injected dose, BMI and scanner type on NECR and image noise in PET imaging. Physics in Medicine & Biology, 56, 5275-5285.

[18] Jacobs, F., Thierens, H., Piepsz, A., Bacher, K., Van de Wiele, C., Ham, H. and Dierckx, R.A. (2005). Optimised tracer-dependent dosage cards to obtain weight-independent effective doses. European Journal of Nuclear Medicine and Molecular Imaging, 32, 581-588.

[19] Lassmann, M., Biassoni, L., Monsieurs, M., Franzius, C. (2008). The new EANM paediatric dosage card: additional notes with respect to F-18. European Journal of Nuclear Medicine and Molecular Imaging, 34, 796-798.

[20] Treves, S.T., Davis, R.T. and Fahey, F.H. (2008). Administered Radiopharmaceutical Doses in Children: A Survey of 13 Pediatric Hospitals in North America. Journal of Nuclear Medicine, 49(6), 1024-1027.

[21] Stauss, J., Franzius, C., Pfluger, T., Juergens, K.U., Biassoni, L., Begent, J., Kluge, R., Amthauer, H., Voelker, T., Hojgaard, L., Barrington, S., Hain, S., Lynch, T. and Hahn, K. (2008). Guidelines for 18F-FDG PET and PET-CT imaging in paediatric oncology. European Journal of Nuclear Medicine and Molecular Imaging, 35, 1581-1588.

[22] Alessio, A.M., Kinahan, P.E., Manchanda, V., Ghioni, V., Aldape, L. and Parisi, M.T. (2009). Weight-Based, Low-Dose Pediatric Whole Body PET/CT Protocols. Journal of Nuclear Medicine, 50(10), 1570-1578.

[23] Alessio, A.M., Sammer, M., Phillips, G.S., Manchanda, V., Mohr, B.C. and Parisi, M.T. (2011). Evaluation of Optimal Acquisition Duration or Injected Activity for Pediatric 18F-FDG PET/CT. Journal of Nuclear Medicine, 52(7), 1028–1034.

[24] Boellaard, R., O' Doherty, M.J., Weber, W.A., Mottaghy, F.M., Lonsdale, M.N., Stroobants, S.G., Oyen, W.J.G., Kotzerke, J., Hoekstra, O.S., Pruim, J., Marsden, P.K., Tatsch, K., Hoekstra, C.J., Visser, E.P., Arends, B., Verzijlbergen, F.J., Zilstra, J.M., Comans, E.F.I., Lammertsma, A.A., Paans, A.M., Willemsen, A.T., Beyer, T., Bockisch, A., Schaefer-Prokop, C., Delbeke, D., Baum, R.P., Chiti, A. and Krause, B.J. (2010). FDG PET and PET/CT: EANM procedure guidelines for tumour PET imaging: version 1.0. European Journal of Nuclear Medicine and Molecular Imaging, 37, 181-200.

[25] Gelfand, M.J., Sharp, S.E., Treves, S.T., Fahey, F.H., Parisi, M.T., Alessio, A.M. (2010). Estimated cumulative radiation dose from PET/CT in children with malignancies. Pediatr Radiol, 40, 1712-713.

[26] Accorsi, R., Karp, J.S. and Surti, S. (2010). Improved dose regimen in pediatric PET. Journal of Nuclear Medicine, 51(2), 293-300.

[27] Alessio, A.M., Fahey, F. and Farell, M. (2013). Survey of radiopharmaceutical dosing strategies for bone and PET scans. Journal of Nuclear Medicine, 54 (Supplement 2), 94.

[28] Bailey, D.L., Jones, T., Spinks, T.J. (1991). Noise equivalent count measurements in a neuro-PET scanner with retractable septa. IEEE Trans Med Imaging, 10, p256-260.

[29] Dahlbom, M., Cherry, S.R., Eriksson, L., Hoffman, E.J. and Wienhard, K. (1993). Optimization of PET instrumentation for Brain Activation Studies. IEEE Transactions on Nuclear Science, 40(4), 1048-1054.

[30] Stearns, C.W., Cherry, S.R., Thompson, C.J. (1995). NECR analysis of 3D brain PET scanner designs. IEEE Transactions on Nuclear Science, 42, 1075-1079.

[31] Badawi, R.D., Marsden, P.K., Cronin, B.F. (1996). Optimization of noise-equivalent count rates in 3D PET. Physics in Medicine & Biology, 41, 1755-1776.

[32] Daube-Witherspoon, M.E., Karp, J.S., Casey, M.E. (2001). PET performance measurements using the NEMA NU-2 70-cm long test phantom for PET. IEEE Nuclear Science Symposium Proceedings.

[33] Smith, R.J. and Karp, J.S. (1998). Comparison of clinical performance with standard measures of PET cameras. Nuclear Science Symposium and Medical Imaging Conference Record IEEE, 2, 1208-1213.

[34] Watson, C.C., Casey, M.E., Beyer, T. (2003). Evaluation of clinical PET count rate performance. IEEE Trans Nuclear Science, 50, 1379-1385.

[35] Stearns, C.W. (2003). Estimating an acquisition-specific NEC Curve for PET acquisitions. IEEE Nuclear Science Symposium and Medical Imaging Conference, 4.

[36] Danna, M., Lecchi, M., Bettinardi, V., Gilardi, M.C., Stearns, C.W., Lucignani, G. and Fazio, F. (2006). Generation of the acquisition-specific NEC (AS-NEC) curves to optimize the injected dose in 3D 18F-FDG whole body PET studies. IEEE Transactions on Nuclear Science, 53(1), 86-92.

[37] Boldys, J., Dvorak, J., Skopalova, M. and Belohavek, O. (2012). Monet Carlo simulation of PET images for injection dose optimization. International Journal for Numerical Methods in Biomedical Engineering, 29(9), 988-99.

[38] Karakatsanis, N., Sakellios, N., Tsantillas, N., Dikaios, N., Tsoumpas, C., Lazaro, D., Loudos, G., Schmidtlein, C.R., Louizi, K., Valais, J., Nikolopoulos, D., Malamitsi, J., Kandarakis, J. and Nikita, K. (2006). Comparative evaluation of two commercial PET scanners, ECAT EXACT HR+ and Biograph 2, using GATE. Nuclear Instruments and Methods in Physics Research Section A, 569(2), 368-372.

[39] Schmidtlein, C.R., Kirov, A.S., Nehmeh, S.A., Erdi, Y.E., Humm, J.L., Amols, H.I., Bidaut, L.M., Ganin, A., Stearns, C.W., McDaniel, D.L. and Hamacher, K.A. (2006). Validation of GATE Monte Carlo simulations of the GE Advance/Discovery LS PET scanners. Med Phys 33(1), 198-208.

[40] Gonias, P., Bertsekas, N., Karakatsanis, N., Saatsakis, G., Gaitanis, A., Nikolopoulos, D., Loudos, G., Papaspyrou, L., Sakellios, N., Tsantilas, X., Daskalakis, A., Liaparinos, P., Nikita, K., Louizi, A., Cavouras, D., Kandarakis, I. and Panayiotakis, G.S. (2007). Validation of a GATE model for the simulation of the Siemens biograph 6 PET scanner. Nuclear Instruments and Methods in Physics Research Section A, 571(1-2), 263-266.

[41] National Electrical Manufacturers Association. (2001). NEMA Standards Publications NU 2-2001: Performance Measurements of Positron Emission Tomography, Rosslyn, VA, USA.

[42] Karakatsanis, N., Loudos, G., Parasyris, A., and Nikita, K. (2008a). A simulation study for optimizing the injected dose of clinical PET systems. IEEE International Workshop on Imaging Systems and Techniques (IST), 98 – 103.

[43] Strother, S.C., Casey, M.E. and Hoffman, E.J. (1990). Measuring PET scanner sensitivity:Relating count rates to image signal-to-noise ratios using noise equivalent counts. IEEE Trans Nuclear Science, 37, 783-8.

[44] Watson, C.C. (2004). Count rate dependence of local signal to noise ratio in positron emission tomography,. IEEE Trans Nuclear Science, 51(5), 2670 – 2680.

[45] Karakatsanis, N., Nikita, K.S. (2008c). A study of the parameters affecting minimum detectable activity concentration level of clinical LSO PET scanners. 8th IEEE International Conference on BioInformatics and BioEngineering, 1 – 6.

[46] Jan, S., Santin, G., Strul, D., Staelens, S., Assié, K., Autret, D., Avner, S., Barbier, R., Bardies, M., Bloomfield, P.M., Brasse, D., Breton, V., Bruyndonckx, P., Buvat, I., Chatziioannou, A.F., Choi, Y., Chung, Y.H., Comtat, C., Donnarieix, D., Ferrer, L., Glick, S.J., Groiselle, C.J., Guez, D., Honore, P.F., Kerhoas-Cavata, S., Kirov, A.S., Kohli, V., Koole, M., Krieguer, M., van der Laan, D.J., Lamare, F., Largeron, G., Lartizien, C., Lazaro, D., Maas, M.C., Maigne, L., Mayet, F., Melot, F., Merheb, C., Pennacchio, E., Perez, J., Pietrzyk, U., Rannou, F.R., Rey, M., Schaart, D.R., Schmidtlein, C.R., Simon, L., Song, T.Y., Vieira, J.M., Visvikis, D., Van de Walle, R., Wiers, E., Morel, C. (2004). GATE: a simulation toolkit for PET and SPECT. Physics in Medicine & Biology, 49, 4543-4561.

[47] Jan, S., Benoit, D., Becheva, E., Carlier, T., Cassol, F., Descourt, P., Frisson, T., Grevillot, L., Guigues, L., Maigne, L., Morel, C., Perrot, Y., Rehfeld, N., Sarrut, D., Schaart, D.R., Stute, S., Pietrzyk, U., Visvikis, D., Zahra, N., Buvat, I. (2011). GATE V6: a major enhancement of the GATE simulation platfrom enabling modeling of CT and radiotheraphy. Physics in Medicine & Biology, 56(4), 881-901.

[48] Agostinelli,B. et al. (2003). Geant4-a simulation toolkit. Nuclear Instruments and Methods in Physics Research Section A: Accelerators, Spectrometers, Detectors and Associated Equipment, 506(3), 250-303.

[49] Ivanchenko, V. et al. 2011 Recent Improvements in Geant4 Electromagnetic Physics Models and Interfaces. Progress in Nuclear Science and Technology, 2, 898-903.

[50] Brun, R. and Rademakers, F. (1997). ROOT - An object oriented data analysis framework. Nuclear Instruments and Methods in Physics Research A, 389, 81-86.

[51] Segars, W. (2001). Development and applications of the new dynamic nurbs-based cardiac-torso (NCAT) phantom. PhD Dissertation, The University of North Carolina.

[52] Chawla, S.C., Federman, N., Zhang, D., Nagata, K., Nuthakki, S., McNitt-Gray, M. and Boechat, M.I. (2010). Estimated cumulative radiation dose from PET/CT in children with malignancies: a 5-year retrospective review. Pediatr Radiol, 40, 681-686.

[53] Mueller, J.W. (1973). Dead-time problems. Nuclear Instruments and Methods, 112, 47-57.

[54] Chang, T., Chang, G., Clark, J.W. Jr, Diab, R.H., Rohren, E. and Mawlawi, O.R. (2012). Reliability of predicting image signal-to-noise ratio using noise equivalent count rate in PET imaging. Med Phys, 39(10), 5891-900.

[55] Nagaki, A., Onoguchi, M. and Matsutomo, N. (2011). Patient weight-based Acquisition Protocols to Optimize 18F-FDG PET/CT Image Quality. J Nucl Med Tech, 39(2), 72-76.

[56] Gelfand, M.J., Parisi, M.T. and Treves, S.T. (2011). Pediatric radiopharmaceutical administered doses: 2010 North American consensus guidelines. Journal of Nuclear Medicine, 52(2), 318–322.

[57] Delbeke, D., Coleman, R.E., Guiberteau, M.J., Brown, M.L., Royal, H.D., Siegel, B.A., Townsend, D.W., Berland, L.L., Parker, J.A., Hubner, K., Stabin, M.G., Zubal, G., Kachelriess, M., Cronin, V. and Holbrook, S. (2006). Procedure guideline for tumor imaging with 18F-FDG PET/CT 1.0. Journal of Nuclear Medicine, 47(5), 885-895.

[58] Federman, N. and Feig, S.A. (2007). PET/CT in evaluating pediatric malignancies: a clinician's perspective. Journal of Nuclear Medicine, 48(12), 1920-2.

[59] Brix, G., Lechel, U., Glatting, G., Ziegler, S., Munzing, W., Muller, S. and Beyer, T. (2005). Radiation exposure of patients undergoing whole-body dual-modality FDG PET/CT examinations. Journal of Nuclear Medicine, 46(4), 608-613.

[60] Pfannenberg, A., Aschoff, P., Brechtel, K., Muller, M., Bares, R., Paulsen, F., Scheiderbauer, J., Friedel, G., Claussen, C. and Eschmann, S. (2007). Low dose non-enhanced CT versus standard dose contrast-enhanced CT in combined PET/CT protocols for staging and therapy planning in non-small cell lung cancer. European Journal of Nuclear Medicine and Molecular Imaging, 34, 36-44.

[61] Zaidi, H., Mawlawi, O. and Orton, C.G. (2007). Simultaneous PET/MR will replace PET/CT as the molecular multimodality imaging platform of choice. Med Phys, 34(5), 1525-1528.

[62] von Schulthess, G.K. and Schlemmer, H.W. (2009). A look ahead: PET/MR versus PET/CT. European Journal of Nuclear Medicine and Molecular Imaging, 36(Suppl 1), S3-S9.

[63] Pichler, B.J., Kolb, A., Nagele, T. and Schlemmer, H.W. (2010). PET/MRI: Paving the way for the next generation of clinical multimodality imaging applications. Journal of Nuclear Medicine, 51(3), 333-336.